Digital Signal Processing 127 (2022) 103409

Contents lists available at ScienceDirect

Digital Signal Processing

www.elsevier.com/locate/dsp

Adaptive M-ary spread spectrum based dual-function detection and communication system

Wei Men [a,b,c], Liang Zhang [a,b,c], Jingwei Yin [a,b,c,*], Jiaqi Wang [a,b,c]

[a] Acoustic Science and Technology Laboratory, Harbin Engineering University, Harbin 150001, China
[b] Key Laboratory of Marine Information Acquisition and Security, Harbin Engineering University, Ministry of Industry and Information Technology, Harbin 150001, China
[c] College of Underwater Acoustic Engineering, Harbin Engineering University, Harbin 150001, China

ARTICLE INFO

Article history:
Available online 21 February 2022

Keywords:
Integrated underwater detection-communication
Adaptive M-ary spread spectrum modulation
Generalized sinusoidal frequency modulated waveform
Genetic algorithm

ABSTRACT

In this paper, we propose a joint detection-communication technique for continuous active sonar (CAS) systems. Particularly, we embed information in the waveforms used for sonar detection via the adaptive M-ary Spread Spectrum modulation, enabling simultaneous communication-detection. To improve the overall performance of the integrated system, we apply the Generalized Sinusoidal Frequency Modulated waveforms and optimize it through the Genetic Algorithm. The numerical simulation and field experimental results show that the proposed technique can perform the CAS detection and communication simultaneously with remarkable reliability.

1. Introduction

Underwater communication and detection are two extremely important underwater information techniques [1–3], and they are usually used as two independent devices. With the rapid development of science and technology, underwater combat methods are constantly developing towards informatization and systemization [4,5]. Failure to have the detection function while communicating will reduce the platform's perception capabilities and threaten its own security. The absence of communication content in the detection signal will weaken the collaboration between platforms. Therefore, the integration of underwater detection and communication (IUDC) becomes increasingly necessary. The IUDC systems can also reduce equipment costs and improve spectrum utilization. As illustrated in Fig. 1, the dual-function waveform (it can simultaneously perform two functions: target detection and communication) transmitted by the active node (i.e., the integrated platform) on the water surface can simultaneously communicate with the underwater hidden communication node and detect the enemy targets, which greatly improves the efficiency of the system. However, the IUDC technology has not yet been widely applied due to the complicacy of the UWA channels, such as large multi-path delay and severe Doppler frequency deviation [6,7]. It is also for these reasons that many methods of dual-function radar-communication systems cannot be applied directly in underwater scenarios.

Generally, the working pattern in an integrated system can be divided into three types: time-sharing systems, beam-splitting systems, and simultaneous systems. Comparing with the first two systems, the simultaneous systems have the highest degree of integration but is the most difficult to achieve [8]. Currently, most of the work on IUDC systems and radar-communication systems is carried out around the simultaneous systems, among which the waveform design is the key research content [9–12]. Maximizing the information entropy embedded into the transmitted waveform is a main task for communication. However, the coherent and restrictive form is required for the active sonar waveform to obtain a pulse compression gain to enhance the detection performance. Thus, an IUDC waveform that simultaneously performs detection and communication functions should have the above two characteristics. Due to this difficulty, most existing works on IUDC systems are premature.

The waveform design of the IUDC system is in its infancy, and related work has been reported. Lu from Northwestern Polytechnical University made a comparative analysis on the detection performance of three commonly used UWA single-carrier communication signals, including minimum-shift keying, two-frequency frequency-shift keying, and binary phase-shift keying [8]. The results provide instruction for the waveform design of the IUDC system. Yin from Harbin Engineering University realizes the continu-

* Corresponding author at: Acoustic Science and Technology Laboratory, Harbin Engineering University, Harbin 150001, China.
E-mail address: yinjingwei@hrbeu.edu.cn (J. Yin).

https://doi.org/10.1016/j.dsp.2022.103409
1051-2004/

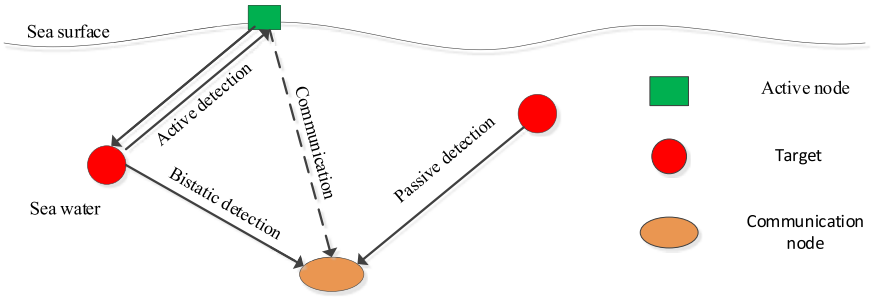

Fig. 1. The schematic diagram of the working scenario of the IUDC system.

ous active sonar-based IUDC (CAS-IUDC) by combining BPSK modulation and Generalized sinusoidal frequency-modulated (GSFM) signal [13], which has a high communication rate and excellent resolution, but the communication performance of the integrated system is greatly affected by the multipath channel.

To improve the continuity of trace trajectory for moving target, it is necessary to increase the target revisit rate (TRR) for active sonars. An obvious shortcoming of traditional pulse active sonar (PAS) is its low detection efficiency, in other words, low TRR. One solution is to continuously transmit detection signals and receive target echoes to achieve continuous target detection. The CAS-IUDC system can not only improve the efficiency of target detection, but also greatly increase the communication rate with friendly nodes due to the reduction of the duty cycle. However, it is difficult to find suitable waveform trains for CAS-IUDC system. Literature [14–16] uses a Linear Frequency Modulated (LFM) signal with long duration T and large swept bandwidth B. The CAS system processes the received target echo signal through N bandpass filters, which reduces the length of each sub-pulse to T/N, the bandwidth to B/N, thereby decreasing the time bandwidth product (TBP) and reducing the processing gain of matched filtering.

To solve the problem, Literature [17] proposed the GSFM waveform, which could generate orthogonal pulses with low-mutual interference by changing the parameters or frequency reflection (FR), and they occupy the same frequency band. Literature [13] prove the GSFM waveform has an approximately thumbtack mainlobe and low sidelobe in ambiguity function (AF) and excellent reverberation suppression performance, and can be applied to the CAS system. However, Literature [18,19] indicated that it is difficult to use parameter variations to identify orthogonal GSFM pulses since the parameters of orthogonal GSFM pulses are hard to determine. The number of orthogonal GSFM pulses generated based only on FR is not enough to support the CAS system. Therefore, a numerical method with the high computational complexity has to be used to resolve the parameters to generate the orthogonal GSFM pulses. In this paper, we use the genetic algorithm (GA) to optimize the parameters of the GSFM pulses by constructing a suitable cost function (CF). The CF takes into account both UWA communication and CAS detection, enabling the application of GSFM in CAS-IUDC systems.

Comparing with the traditional chip spread spectrum modulation, the M-ary Spread Spectrum modulation provides a higher communication rate and frequency band efficiency [20,21], since it exploits the waveform orthogonality. However, as the modulation order increases, the required waveforms for conventional M-ary Spread Spectrum modulation increase exponentially, which brings a huge challenge to waveform selection. To alleviate this issue, we propose an adaptive M-ary Spread Spectrum (AMSS) modulation scheme, which requires only a small amount of orthogonal waveforms to achieve a communication rate equivalent to that of the conventional schemes. To avoid affecting the target detection capability of the CAS system, we also propose a CAS-IUDC method based on AMSS modulation (CAS-IUDC-AMSS), which can carry digital information by encoding each sub-pulse of the CAS system. The sub-pulses transmitted by the CAS-IUDC-AMSS system are designed to be independent to reduce the mutual interference between them when detecting multiple targets. At the communication receiving end, an M-ary energy detector (MED) algorithm with low computational complexity is used to decode the received signal without requiring channel equalization; at the integrated platform receiving end, traditional array processing techniques are used to estimate various parameters of the target, including distance, speed, and azimuth. In addition to the computer simulations, we also conducted a field experiment on proposed integrated system to examine its communication performance, which took place in Songhua River, HeiLongjiang Province, China. The results validate the effectiveness of the CAS-IUDC-AMSS algorithm.

The contributions of this paper are summarized as follows:

- An underwater dual-function transmit waveform is designed based on CAS system.
- The AMSS modulation method is proposed to enable sub-pulses of CAS system to carry information.
- The parameters and FRs of GSFM waveforms are optimized based on the GA to improve the communication and detection performance of the integrated system.

The remainder of this paper is organized as follows. Section 2 introduces the model of CAS-IUDC-AMSS system, Section 3 reviews the GSFM signal and its characteristics, and Section 4 describes the Optimization of the GSFM waveform trains. Section 5 presents the simulation results, Section 6 provides the field experiment results. Finally, Section 7 concludes the paper.

2. CAS-IUDC-AMSS system

2.1. Transmitter

A CAS system constantly transmits signals into the medium and collects echoes from interested targets. Fig. 2 shows the schematic diagram of the transmitted signal in the CAS system. The waveforms are collections of pulses transmitted sequentially, which can be expressed as

$$s(t) = \frac{1}{\sqrt{N \cdot T_{PRI}}} \sum_{n=0}^{N-1} s_n (t - nT_{PRI}) \tag{1}$$

where N is the number of sub-pulses, T_{PRI} is the pulse repetition period, and it also is the pulse width in a CAS system, $\frac{1}{\sqrt{N \cdot T_{PRI}}}$ normalizes the energy of the waveform train, and $s_n(t)$ is n-th sub-pulse, which can be expressed as

$$s_n(t) = \frac{\mathrm{rect}(t)}{\sqrt{T}} e^{j\varphi_n(t)} e^{j2\pi f_n t} \tag{2}$$

where rect(t) is the rectangular envelope of the pulse, and f_n and $\varphi_n(t)$ are the center frequency and the phase modulation function of the n-th sub-pulse, respectively.

To maintain the target detection performance while enabling the signal transmitted by CAS system to complete the two tasks of target detection and communication simultaneously, all subpulses in CAS are coded by M-ary Spread Spectrum to carry information. Since the CAS-IUDC-AMSS system only transmits the specified pulse train waveforms used for active sonar detection, as long as a sufficient number of pulse waveforms are available, its detection performance will not be affected.

We provide two M-ary Spread Spectrum coding schemes. Fig. 3 shows the flow charts of coding scheme 1. To reduce the mutual-interference between sub-pulses, we preset a waveform train for each sub-pulse, forming a collection of N waveform trains. Each waveform train contains M pulse waveforms, thus a sub-pulse can carry $\log_2 M$ bits of information after coding. Firstly, the binary data stream is converted from serial to parallel, where each $\log_2 M$ bits information is divided into a group. The grouped information then decides the pulse waveform to be selected from specific sub-pulse waveform train. Finally, parallel to serial conversion is performed to obtain an integrated waveform. Assuming the CAS system need to transmit N sub-pulses to detect the target, coding scheme 1 requires a total of N waveform trains, that is, $M \cdot N$ orthogonal waveforms. The process of the second coding scheme, namely, the AMSS, is illustrated in Fig. 4. Similarly,

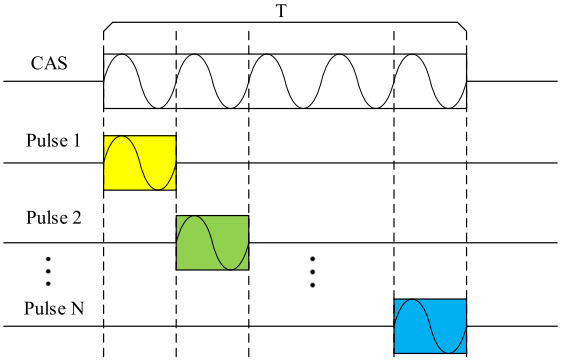

Fig. 2. The schematic diagram of the transmitted signal in the CAS system.

the binary data stream is converted from serial to parallel, and the modulated by the AMSS. To reduce the mutual-interference from sub-pulses, we need to update waveform train 1 by waveform train 2 after completing each modulation, such that the waveforms used in the AMSS modulation of N times are distinct. To achieve the same communication rate as scheme 1, scheme 2 only needs two waveform trains, that is, $M + N - 1$ orthogonal waveforms. In the case of different values of N and M, the comparison of the number of waveforms required by the two schemes is given as:

$$\begin{cases} M + N - 1 = M \cdot N, \mathrm{M} = 1 \text{ or } \mathrm{N} = 1 \\ M + N - 1 < M \cdot N, \text{ else} \end{cases} \tag{3}$$

In CAS systems, N should be greater than 1, when $N = 1$, it is a PAS system. When $M = 1$, the digital information carried by each sub-pulse is $\log_2 M = 0$ bits, so the value of M in M-ary spread spectrum modulation should be no less 2. Therefore, the number of orthogonal waveforms required for encoding scheme 2 (AMSS modulation) is less than that of encoding scheme 1. And the gap will grow larger when M and N increase.

2.2. Receiver

Fig. 5 shows the processing flow of the received signal in the communication node and the integrated platform. The transmitted signal reaches the communication node through the ocean channel. At the communication receiving end, the signal is band-pass filtered, and then the information carried by each sub-pulse is decoded. Assume that the received signal processed by band-pass filtering is

$$r_c(t) = \int_{-\infty}^{\infty} h(\tau) s(t - \tau) d\tau + n_c(t) \tag{4}$$

where $h(\tau)$ is the impulse response function of the UWA multi-path channel and $n_c(t)$ is additive white Gaussian noise (AWGN) received by the communication node. The MED algorithm is used to decode the n-th sub-pulse of the transmitted signal, the output energy vector can be expressed as:

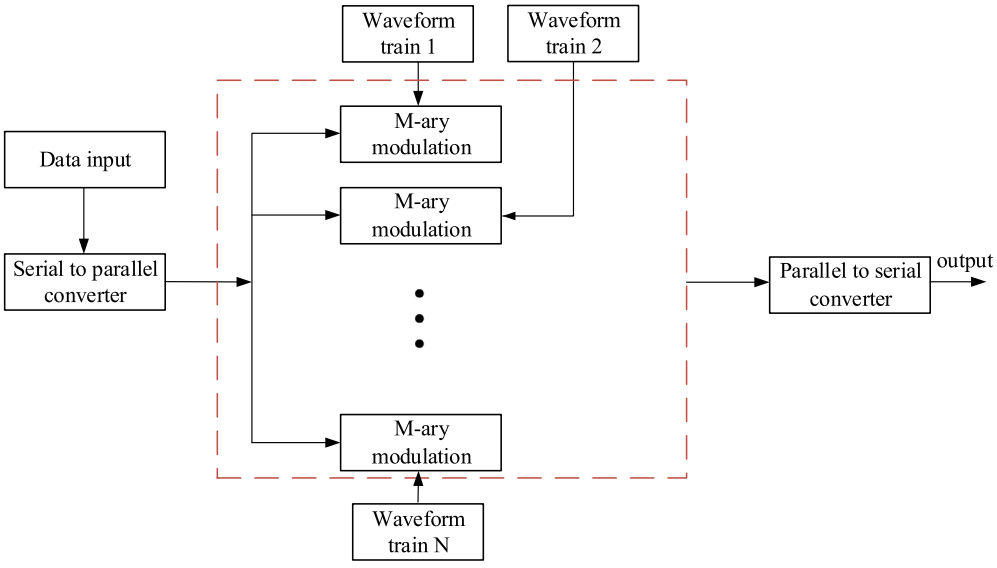

Fig. 3. Flow chart for coding scheme 1.

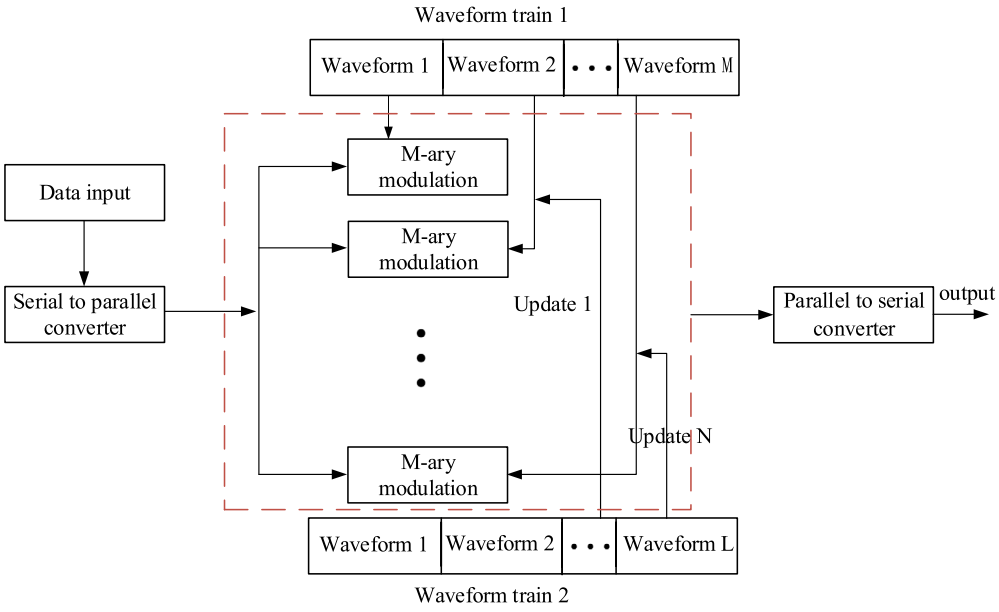

Fig. 4. Flow chart for coding scheme 2.

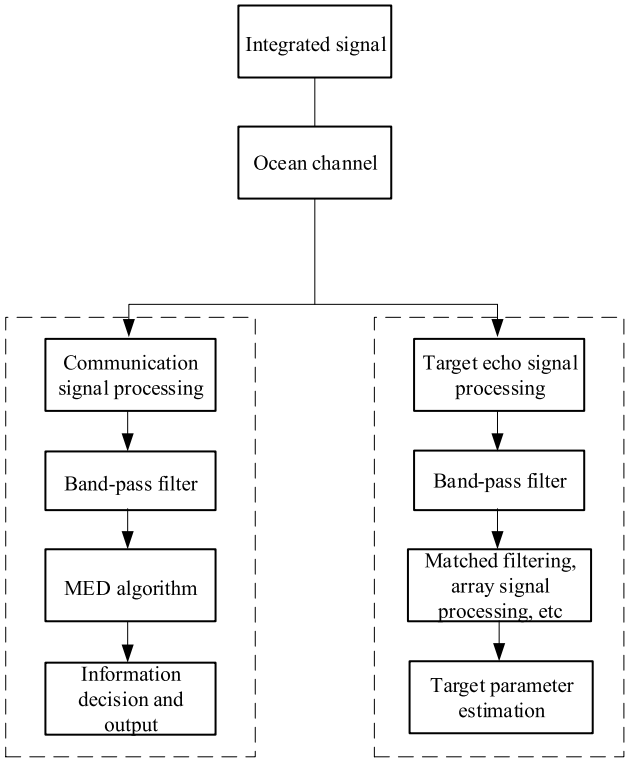

Fig. 5. The processing flow of the received signal.

$$\begin{aligned} E_n(\lambda) &= \left|\mathbf{S}_n^T r_n\right|^2 \\ &= \left|\mathbf{S}_n^T s_n + \mathbf{S}_n^T n_c\right|^2 \\ &= \left[\left|s_1^T s_n\right|^2, \left|s_2^T s_n\right|^2, \cdots, \left|s_M^T s_n\right|^2\right]^T \end{aligned} \tag{5}$$

where $1 \le \lambda \le M$ and S_n is the pulse waveform matrix of the CAS system when decoding the n-th sub-pulse. For the AMSS modulation, S_n needs to be updated after completing each decoding process. $\mathbf{S}_n^T n_c$ is the noise component after spread spectrum processing, and in most cases its value is small and even can be ignored. Then, the information can be obtained by searching the maximal of the energy output:

$$b_n = \arg\max_{\lambda} \{E_n(\lambda)\} \tag{6}$$

Assume a total of L targets are located in the far-field, the signal touches the targets and returns to the receiving end of the integrated platform, which can be expressed as:

$$y_r = \sum_{l=1}^{L} A_l \int_{-\infty}^{\infty} h_l(\tau_l) s\left(t-\tau_l\right) e^{j2\pi\delta_l} d\tau_l + n_t(t) \tag{7}$$

where A_l is the amplitude of the l-th echo signal, with h_l being the corresponding channel impulse response. τ_l and δ_l are the delay and the Doppler deviation of the l-th target, respectively. n_t is the environmental noise at the integrated platform.

Since the detection scheme of the proposed CAS-IUDC-AMSS system is the same as the original CAS system, the traditional CAS target detection algorithm is directly used to process the received signal in Eq. (7). As shown in Fig. 5, band-pass filter, matched filter, array signal processing and other techniques are used in a sequence to enable estimation of target parameters. In the sonar systems, matched filter is the most commonly used receiver algorithms for target detection in AWGN. If the target is relatively stationary to the transmitter and receiver, the target echo can match with the transmitted IUDC signal at some certain time delay. However, if the target moves, the Doppler effect will occur, causing the signal to be stretched or compressed in the time domain. If the relative speed of the target and the integrated platform is v, the Doppler scaling factor is:

$$\eta = \frac{1+v/c}{1-v/c} \tag{8}$$

where c is the sound speed in water.

The receiver perform matched filtering at different time delays and Doppler scaling factors to detect presence of targets. It is well known that the detection performance could be measured by the AF function. The AF between the m-th and n-th sub-pulse at time delay τ and Doppler scaling factor η is:

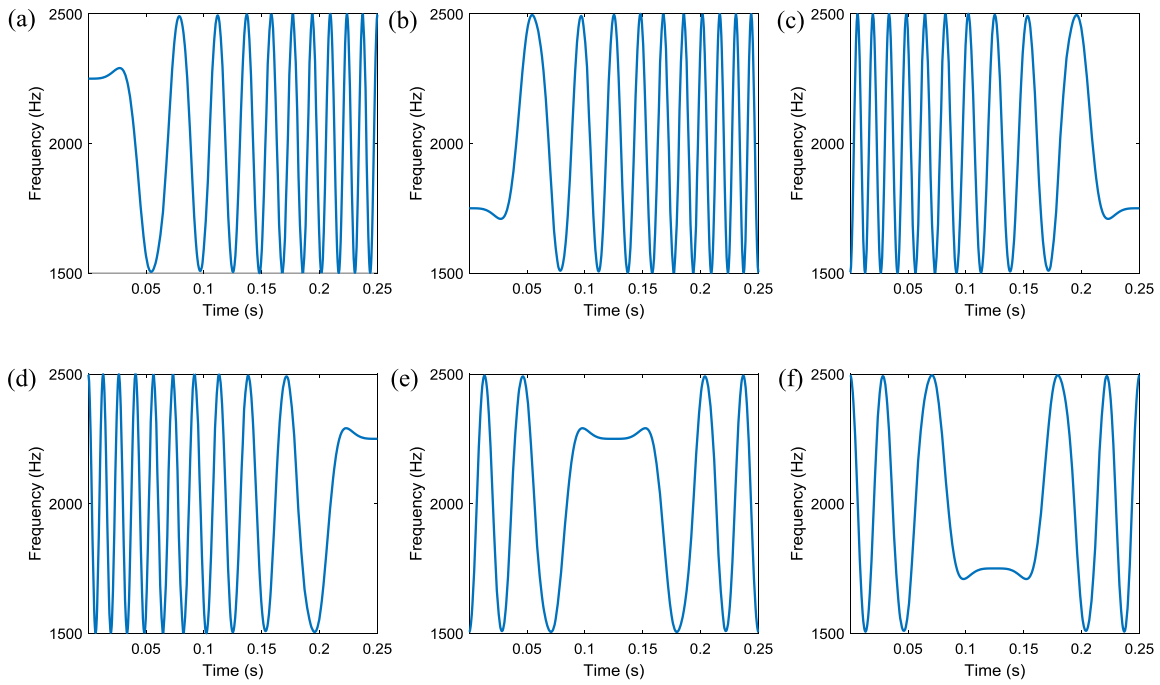

Fig. 6. Instantaneous frequency of six FRs with (a) Forward-Time (b) Forward-Time/Flipped-Frequency (c) Reverse-Time (d) Reverse-Time/Flipped-Frequency (e) Even-symmetric and (f) Even-symmetric/Flipped-Frequency.

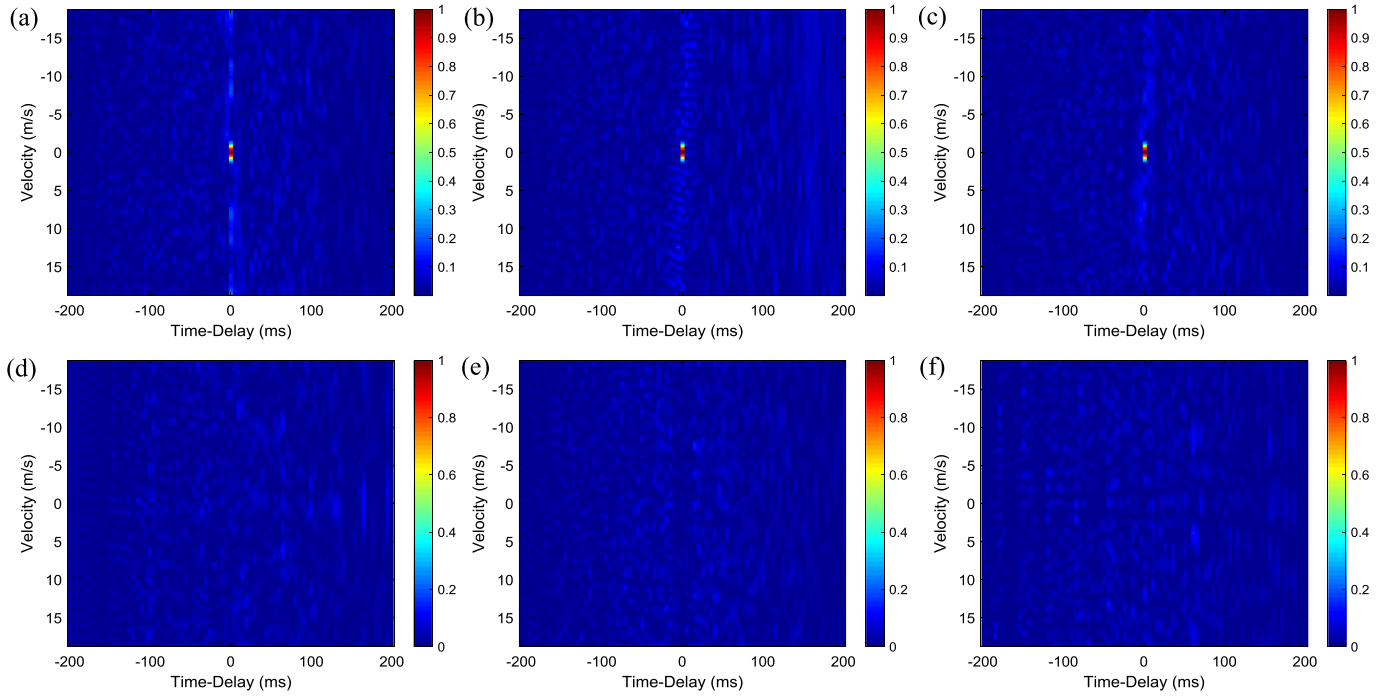

Fig. 7. The BAAF of (a) GSFM1 (b) GSFM2 and (c) GSFM3, and the BCAF between (d) GSFM1 and GSFM2 (e) GSFM1 and GSFM3 (f) GSFM2 and GSFM3.

$$\chi_{m,n}(\tau,\eta)=\sqrt{\eta}\int s_m(\mathrm{t})s_n^*(\eta(\mathrm{t}-\tau))dt \tag{9}$$

3. GSFM signal and its characteristics

As illustrated in Section 2, it is quite difficult for the integrated system to find enough waveforms that are nearly orthogonal to each other and suitable for CAS detection. The LFM signals and hyperbolic frequency modulation signals need to partition the frequency bands to generate pulses orthogonal to each other. That causes the frequency spectrum utilization to be extremely low, and is prohibited by the narrowness of the underwater spectrum. Due to its excellent time-frequency resolution and ability to generate a large number of near-orthogonal waveforms at the same frequency band, the GSFM signal is utilized in the CAS System.

The waveform expression of GSFM signal can be described as

$$g(t)=\frac{\mathrm{rect}(t)}{\sqrt{T_g}}e^{j\varphi_{GSFM}(t)}e^{j2\pi f_c t} \tag{10}$$

where T_g is the pulse width, f_c is the center frequency, $\varphi_{GSFM}(t)$ is the phase modulation function, expressed as:

$$\varphi_{GSFM}(t) = \frac{\beta}{t^{(\rho-1)}} \sin\left(\frac{2\pi\alpha t^{\rho}}{\rho}\right) \tag{11}$$

where β is the modulation index, and $\beta = B/2\alpha$, B is the bandwidth. α is a frequency modulation term. ρ is a dimensionless parameter that must be greater than or equal to 1. When it is equal to 1, the GSFM signal degenerates into a sinusoidal frequency-modulated signal. GSFM waveforms with different parameters α and ρ can be almost orthogonal to each other. FR technology can further increase the number of nearly orthogonal GSFM waveforms. As shown in Fig. 6, the six FRs can generate six waveforms that occupy the same frequency band and are nearly orthogonal to each other, and they all have a thumbtack auto-AF.

The broadband auto-AF (BAAF) and the broadband cross-AF (BCAF) of the GSFM signals is given in Fig. 7. All the GSFM signals have a pulse length $T_g = 0.25$ s, center frequency $f_c = 2$ kHz, bandwidth $B = 2$ kHz, and parameters $\rho = 2$, $\alpha = 160\ s^{-2}$. Fig. 7 (a), (b) and (c) show the BAAF of the GSFM signals, where GSFM1 represents the GSFM signal with an instantaneous frequency (IF) of Forward-Time as shown in Fig. 6 (a), GSFM2 represents the GSFM signal with an IF of Reverse-Time as shown in Fig. 6 (b), and GSFM3 represents the GSFM signal with an IF of Forward-Time/Flipped-Frequency as shown in Fig. 6 (c). It can be seen that GSFM signals with different IFs have a high range and velocity resolution. Fig. 7 (d), (f) and (e) shows the BCAF of the GSFM1, GSFM2 and GSFM3. The peak value of BCAF is very low due to the near-orthogonality between the waveforms, which indicates that the cross-correlation level is low at any Doppler shift and time delay, thereby being able to provide a good separation performance. In the CAS system, it's beneficial to target detection when the BAAF of waveforms have a high peak sidelobe level and the BCAF of waveforms have a low mainlobe level.

Reverberation is one of the main factors that limit the effectiveness of active sonar target detection in a shallow sea environment [22–24]. Traditional active sonar signals such as continuous wave (CW) signals and LFM signals have poor detection performance in the reverberant background. Assuming that the reverberation scatterer is stationary and evenly distributed with equal intensity along the distance, the reverberation intensity of matched filter output under different Doppler can be expressed in the form of a Q-function:

$$Q(\eta) = \int_{-\infty}^{\infty} |\chi(\tau, \eta)|^2 d\tau \tag{12}$$

The smaller the Q function is, the smaller the reverberation output of the transmitted signal is, and the more beneficial it is for target detection.

Fig. 8 shows the Q function distribution for a GSFM signal and three commonly used active sonar signals (i.e., CW, LFM and pseudo-noise signals). The parameters in Fig. 8 are the same as Fig. 7. It can be seen that the anti-reverberation ability for the GSFM signal is significantly better than for the CW and LFM signals. Moreover, GSFM signals are the best among the four waveforms in terms of anti-reverberation for low-speed targets, while for high-speed targets, GSFM signals are only slightly worse than pseudo-noise signals.

In summary, in view of the nearly orthogonality, high distance and speed resolution, and strong anti-reverberation performance of GSFM signals, they are suitable for the proposed CAS-IUDC-AMSS system. However, the performance of GSFM waveforms obtained by changing the parameters and the FR technology is uneven. Therefore, we need an optimization method to find the $M+N-1$ GSFM waveforms with the best performance.

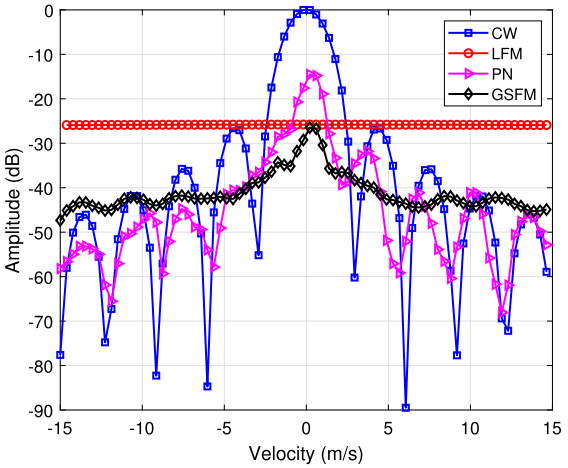

Fig. 8. Q function distribution diagram for different signals.

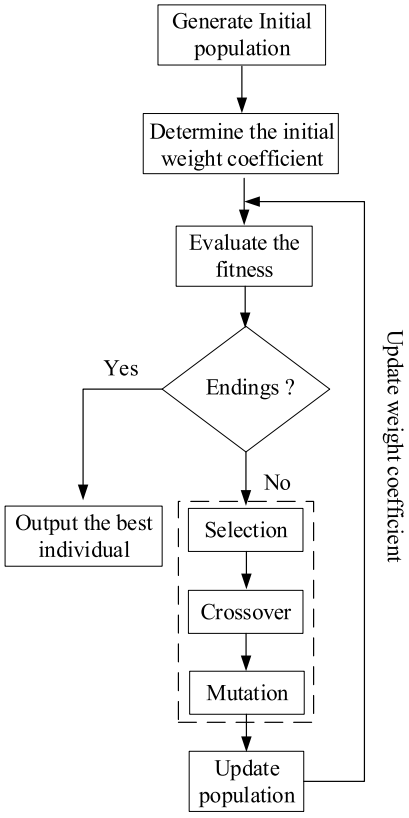

Fig. 9. The flow chart for GA processing.

4. Optimization of the GSFM waveform trains based on GA

GA is a global optimization algorithm that simulates Darwin's biological evolution theory, and it is one of the most commonly used algorithms in current signal optimization design [25,26]. To improve the performance of the CAS-IUDC-AMSS system, this paper uses GA to optimize the parameters α and ρ and FRs of the GSFM pulse trains. The flow chart for GA processing is shown in Fig. 9. The main operations of GA include: chromosome coding, initial population setting, evolution algebra setting, crossover probability and mutation probability setting, fitness function calculation, selection, crossover and mutation, etc. Several individuals were randomly generated in the feasible region as the initial population. The crossover probability represents the probability that the

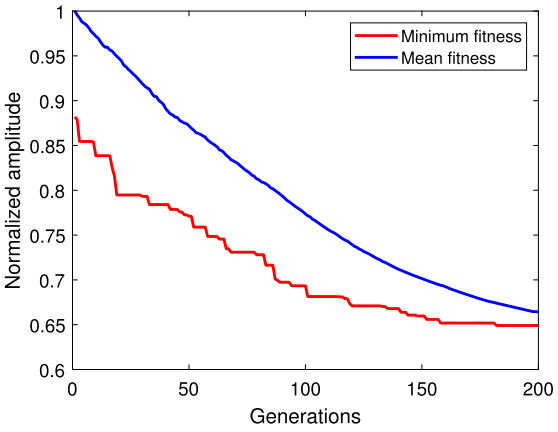

Fig. 10. The minimum fitness and mean fitness of the population with various generations.

offspring individuals generated by crossover operation are inherited to the next generation. The greater the crossover probability, the greater the probability that the offspring will be inherited to the next generation. Mutation probability represents the probability of chromosome gene mutation. Generally, the value is very small. Mutation makes the genetic algorithm have local random search capability while ensuring group diversity. The role of genetic operators (including selection, crossover, mutation) is to operate on the current population to produce the next generation of population. It is a key issue to construct an appropriate CF for waveform optimization using GA.

Assuming the waveform train model to be optimized is:

$$G_m = [g_1, g_2, \cdots g_{M+N-1}] \tag{13}$$

we need to define a CF to calculate the fitness of the chromosomes under each generation in the GA. The design of the CF needs to take into account the performance improvement of two aspects, namely, the CAS detection and AMSS-based communication.

Assuming that the number of sampling points after discretization of each GSFM pulse is D, the auto-correlation and cross-correlation function of the pulses can be defined as:

$$R(v, w, k) = \begin{cases} \frac{1}{D}\sum_{d=1}^{D-k} g_v(d) g_w(d+k), 0 \le k < D \\ \frac{1}{D}\sum_{d=-k+1}^{D} g_v(d) g_w(d+k), -D < k < 0 \end{cases} \tag{14}$$

where $v, w = 1, 2, \cdots, M+N-1$ and K is a discrete time index.

The ideally orthogonal waveforms should satisfy:

$$R(v, v, k) = \begin{cases} 1, k = 0 \\ 0, k \neq 0 \end{cases} \tag{15}$$

and

$$R(v, w, k) = 0, -D < k < D, v \neq w \tag{16}$$

Eq. (15)–(16) indicates that, idealistically, the auto-correlation function should be an unit impulse response function, and the cross-correlation function should be 0 everywhere. However, according to law of conservation of energy, it is impossible for us to find out plenty of orthogonal waveforms, the quasi-orthogonal waveforms are available. Thus, the normalized sidelobe of the auto-correlation function in Eq. (15) can be expressed as:

$$AS(v) = [R(v, 1), R(v, 2), \cdots, R(v, \mathrm{D}-1)]/R(v, 0) \tag{17}$$

The cross-correlation function in Eq. (17) can be expressed as:

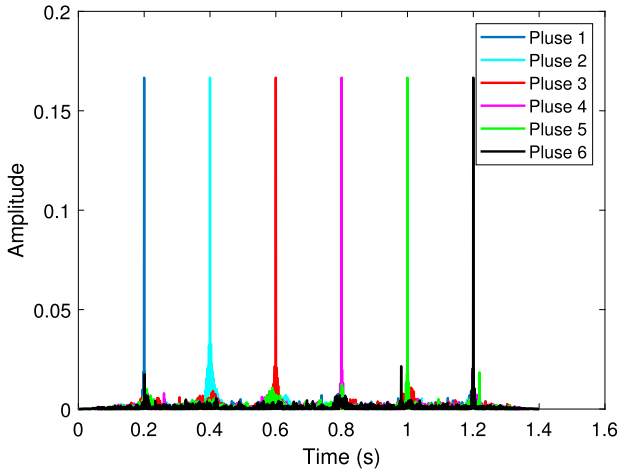

Fig. 11. Matched filtering results.

$$C(v, w, k) = [R(v, w, -D+1), R(v, w, -D+2), \cdots, R(v, w, \mathrm{D}-1)]/R(v, 0) \tag{18}$$

The sidelobe peak of auto-correlation (SPAC) of all pulses in G_m can be defined as:

$$SPAC = \sum_{v=1}^{M+N-1} \max_k |AS(v, k)| \tag{19}$$

The peak of cross-correlation (PCC) of all pulses in G_m can be defined as:

$$PCC = \sum_{i=1}^{M+N-1} \sum_{w=v+1}^{M+N-1} \max_k |C(v, w, k)| \tag{20}$$

Accordingly, the fitness function for the SPAC and PCC can be given as:

$$F_1 = \min_{\Omega}(SPAC + PCC) \tag{21}$$

where Ω represents the parameters α and ρ and FRs of the GSFM pulses.

The sidelobe level of Auto-AF (SLAA) is defined as the ratio of the maximum sidelobe to the main lobe. In active sonar, greater SLAA of the transmitted signal means lower resolution, so the SLAA optimization is to improve the resolution of the integrated signal. The SLAA of all pulses in G_m can be defined as:

$$SLAA = \sum_{v=1}^{M+N-1} \frac{\chi_v(\tau_1, \eta_1)}{\chi_v(0, 0)} \tag{22}$$

where $\chi_v(\tau_1, \eta_1)$ represents the maximum sidelobe of the Auto-AF.

The mainlobe level of cross-AF (MLCA) is defined as the maximum value of the cross-AF. To reduce mutual interference between sub-pulses in the CAS system, the MLCA should be suppressed as much as possible. The MLCA of any two pulses in G_m can be defined as:

$$MLCA = \sum_{v=1}^{M+N-1} \sum_{w=v+1}^{M+N-1} \max \left| \frac{\chi_{v,w}(\tau, \eta)}{\chi_v(0, 0)} \right| \tag{23}$$

According to the arguments above, the fitness function for the SLAA and MLCA can be given as:

$$F_2 = \min_{\Omega}(SLAA + MLCA) \tag{24}$$

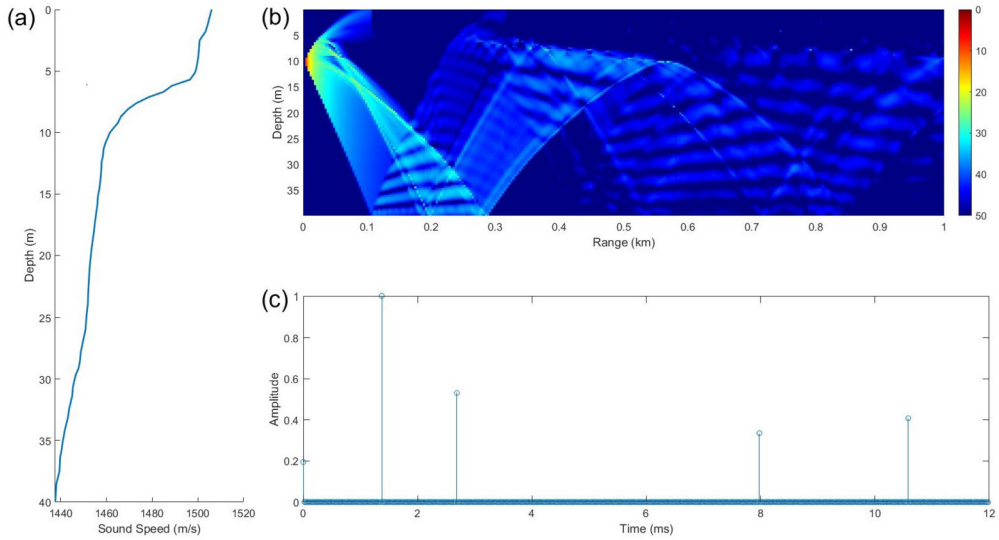

Fig. 12. (a) The measured sound speed profile using a CTD (b) the simulated coherent transmission loss pseudo color map (c) the simulated UWA channel.

In order to improve the anti-reverberation ability of the integrated waveform when detecting low-speed targets, we chose to optimize the Q function of all pulses in G_m at the low speed regions. Assuming the Doppler scaling factor caused by the low-speed target is within the interval $[-\eta_1 \sim \eta_1]$, the sum of Q functions (SQF) is:

$$SQF = \int_{-\eta_1}^{\eta_1} \int_{-\infty}^{\infty} |\chi(\tau, \eta)|^2 d\tau d\eta \tag{25}$$

The SQF of all pulses in G_m can be defined as:

$$GQ = \sum_{v=1}^{M+N-1} SQF_v \tag{26}$$

So, the fitness function for the SQF can be given as:

$$F_3 = \min_{\Omega}(GQ) \tag{27}$$

Reducing the interference term in Eq. (5) can improve the decoding performance of the MED algorithm at the communication receiving end, the design of waveform trains for the CAS-IUDC-AMSS system should make the cross-energy (CE) between the pulses be as weak as possible. The CE of two pulses can be defined as:

$$CE_{v,w} = \left| S_v^T \cdot S_w \right|^2 \tag{28}$$

Then the sum of CE for any two different pulses in G_m can be defined as:

$$CE = \sum_{v=1}^{M+N-1} \sum_{w=v+1}^{M+N-1} \left| g_v^T \cdot g_w \right|^2 \tag{29}$$

The fitness function for the CE can be given as:

$$F_4 = \min_{\Omega}(CE) \tag{30}$$

According to the above results, the CF of the optimization model is:

$$F(\alpha, \rho, \mathrm{FR}) = \omega_1 \cdot F_1 + \omega_2 \cdot F_2 + \omega_3 \cdot F_3 + \omega_4 \cdot F_4 \tag{31}$$

where $\omega_\lambda (\lambda = 1, 2, 3, 4)$ are the weight coefficients. In this paper, the units of four fitness functions are different, and $F1$, $F2$, $F3$ and $F4$ represent area, area, volume and energy, respectively. Multi-objective GAs are often ineffective for multi-objective tasks [27], as they tend to focus on one target direction, while ignoring the search for other targets, thereby omitting good solutions on other targets. This is due to the unreasonable setting of weight coefficients. We use the average adaptive weight approach to solve this problem, which can increase the population diversity in multi-objective optimization.

For a multi-objective optimization problem with objectives Λ and chromosomes Ψ, the initial (1-th generation) weight coefficients are defined as $\omega_{\lambda,1} = 1/\Lambda, \lambda = 1, 2, \cdots, \Lambda$. To achieve the global objective search, the weight coefficients need to be adjusted adaptively along with evolution. The weight coefficients of the $(p+1)$-th generation can be updated from that of the p-th generation, as follows:

$$w_{\lambda,p+1} = \frac{\frac{1}{\Lambda} \sum_{\lambda=1}^{\Lambda} \overline{F_{\lambda,p}}}{\overline{F_{\lambda,p}}} w_{\lambda,p} \tag{32}$$

where $\overline{F_{\lambda,p}}$ denotes mean fitness of the λ-th objective in the p-th generation, it can be written as:

$$\overline{F_{\lambda,p}} = \frac{1}{\Psi} \sum_{\psi=1}^{\Psi} F_{\lambda,p}\left(x_\psi\right) \tag{33}$$

where $\psi = 1, 2, \cdots, \Psi$. As shown in Fig. 9, the weight coefficients are updated by Eq. (32) after completing each generation of evolution.

Through the GA, we can obtain optimal waveform trains and the corresponding parameters by minimizing the CF Eq. (31). When the fitness of the optimal individual reaches the given threshold, or the fitness of the optimal individual and the mean fitness no longer rise, or the number of iterations reaches the preset number of generations, the GA terminates.

5. Numerical simulation

This section gives numerical simulations to illustrate the performance of our proposed CAS-IUDC-AMSS system. First, the results of GSFM waveform train optimization are given. Second, the communication bit error rate (BER) performance of the integrated system

under the UWA channel is demonstrated, and compared with the LFM signal using sub-band processing. Finally, we examine the detection performance of the CAS-IUDC-AMSS system.

5.1. Optimization of the GSFM pulse trains

For the CAS-IUDC-AMSS system, we consider a GSFM waveform train with sizes $M = 8$, $N = 8$, which contains a total of 16 pulses. All pulses last for a duration $T_g = 0.2$ s. The center frequency is set as $f_c = 1.5$ kHz, and the bandwidth is $B = 1$ kHz, the sampling rate is 10 kHz. The setting of GA is as follows: the initial population contains 80 items, the probability of crossover is 0.8, and the probability of mutation is 0.01. The algorithm iterates 200 generations. Fig. 10 shows the minimum fitness and mean fitness of the population as a function of number of iterations. It can be observed in Fig. 10 that the minimum fitness and mean fitness decreases with the increase of generation. The minimum fitness become stable after 160 iterations, which shows that the optimal individual (i.e., the required number of GSFM waveforms) has been attained. Optimized parameters (α_v, ρ_v and $FR_v, v = 1, 2, \cdots, 16$) of 16 pulses are listed as Table 1, we only used the first four instantaneous frequencies shown in Fig. 6. Fig. 11 shows the matched filtering results of the first 6 sub-pulses in the optimized GSFM pulse train. The nearly orthogonality between the sub-pulses substantially reduces mutual interference, which is beneficial to detection of the CAS-IUDC-AMSS system.

5.2. Communication BER performance

Fig. 12(a) shows the sound velocity profile measured by a conductivity-temperature-depth profiler in the experiment in Songhua Lake, Jilin Province, in July 2019. Fig. 12(b) is the simulated coherent transmission loss pseudo color map, and Fig. 12(c) is the simulated multipath UWA channel between the transmitter and receiver based on Bellhop using the sound speed profile in Fig. 12(a), where the depth of the transmitter is 10 m, and a receiver is deployed at 20 m depth 1 km away. Next, the communication BER performance of the proposed CAS-IUDC-AMSS system will be simulated. We first prove that proposed system has better communication and detection performances over the sub-band LFM signal in Sections 5.2 and 5.3. To obtain 16 sub-pulses, we divide the full-band $1 - 2$ kHz into 8 sub-bands, and the two LFM signals in each sub-band use up-and-down sweeps to achieve orthogonality to each other. Fig. 13 shows the communication BER performance of the CAS-IUDC-AMSS system using two signals as sub-pulses, where a total of 10^4 Monte-Carlo simulations are performed for each BER count. It can be clearly seen that CAS-IUDC-AMSS system with optimized GSFM signal as sub-pulse has a lower BER comparing with the LFM under the same signal-to-noise ratio (SNR). When the SNR is greater than -8 dB, zero BER communication under limited data transmission can be performed.

5.3. Detection performance

The detection performance of the proposed CAS-IUDC-AMSS system was analyzed using Monte-Carlo simulation, Fig. 14 shows

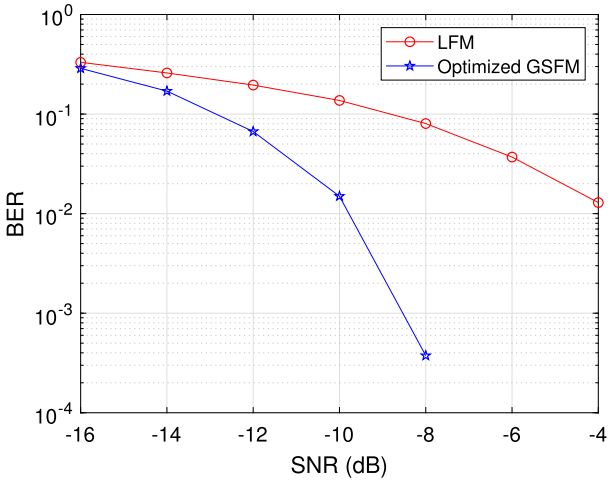

Fig. 13. BER performance of the CAS-IUDC-AMSS system.

Table 1
Optimized parameters of 16 GSFM pulses.

Waveform	α	ρ	FR
Pluse 1	2.347	292.106	3
Pluse 2	2.360	339.988	3
Pluse 3	2.069	337.032	2
Pluse 4	2.561	193.995	2
Pluse 5	2.362	235.033	2
Pluse 6	2.083	224.185	2
Pluse 7	2.252	346.811	2
Pluse 8	2.001	250.362	2
Pluse 9	2.124	331.757	3
Pluse 10	2.106	187.288	3
Pluse 11	2.005	277.805	3
Pluse 12	2.052	327.921	1
Pluse 13	2.060	340.258	3
Pluse 14	2.119	240.033	3
Pluse 15	2.076	315.030	4
Pluse 16	2.343	326.789	2

FR 1: Forward-Time.
FR 2: Forward-Time/Flipped-Frequency.
FR 3: Reverse-Time.
FR 4: Reverse-Time/Flipped-Frequency.

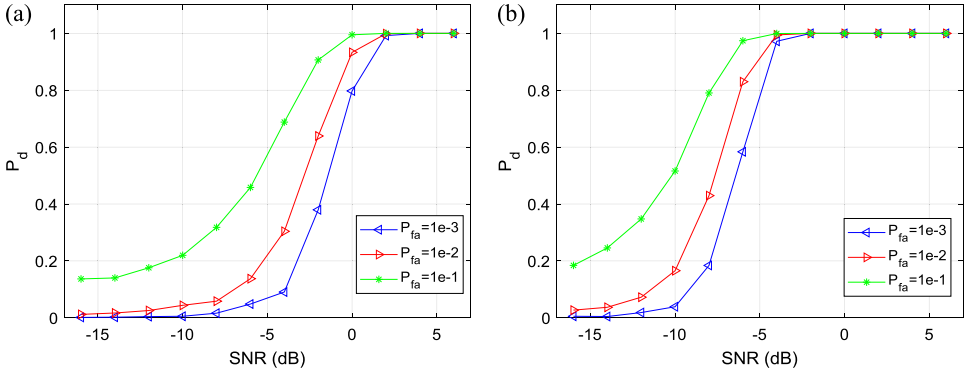

Fig. 14. P_d for various SNR, the integrated system uses (a) sub-band LFM signal, and (b) optimized GSFM signal.

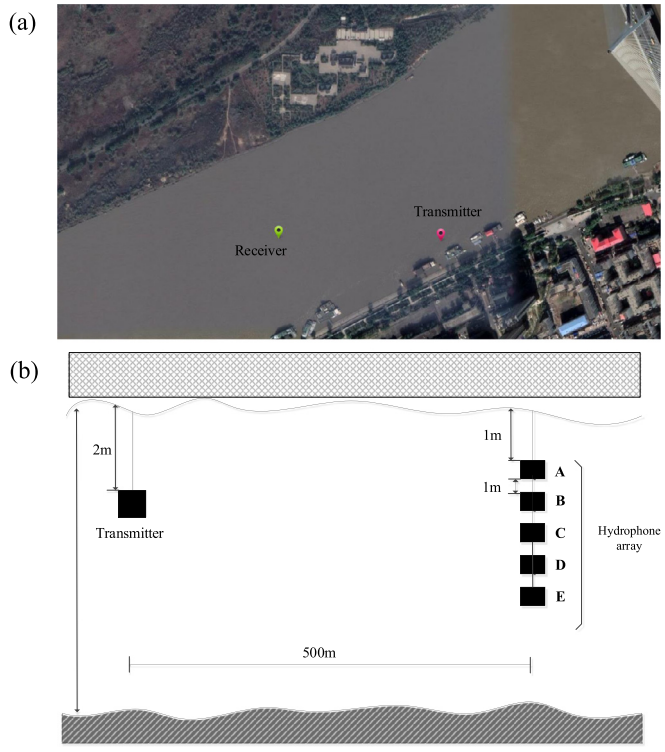

Fig. 15. (a) The satellite image of the experiment scenario, and (b) the specific experiment layout. (For interpretation of the colors in the figure(s), the reader is referred to the web version of this article.)

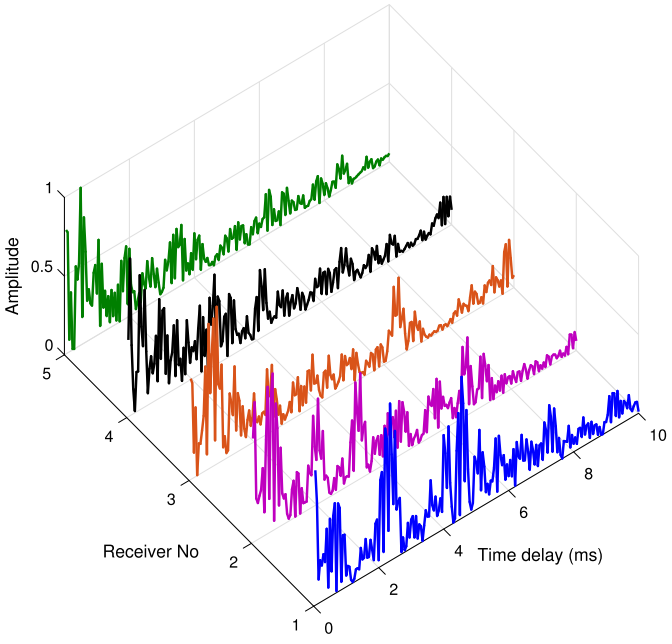

Fig. 16. UWA channel estimation results.

the detection probability of the integrated system based on different signals versus different SNRs. The Fig. 14 (a) and (b) are results corresponding to the sub-band processing LFM signal and the optimized GSFM signal, respectively. The simulation results indicate that the proposed integrated system using the optimized GSFM signal has better detection performance over its LFM counterpart. The probability of detection (P_d) is greater than 90% for all the three false alarm probabilities (P_{fa}) when the SNR is greater than

Table 2
The decoding results.

Receiver	SNR (dB)	Original SER (%)		New SER (%)	
		System I	System II	System I	System II
#A	14.24	0	0	5.00(12/240)	0.42(1/240)
#B	13.18	0	0	0.84(2/240)	0
#C	15.57	0	0	1.67(4/240)	0
#D	15.04	0	0	3.33(8/240)	0
#E	13.97	0	0	1.67(4/240)	0

System I: the CAS-IUDC-AMSS system with sub-band LFM signals.
System II: the CAS-IUDC-AMSS system with optimized GSFM signals.

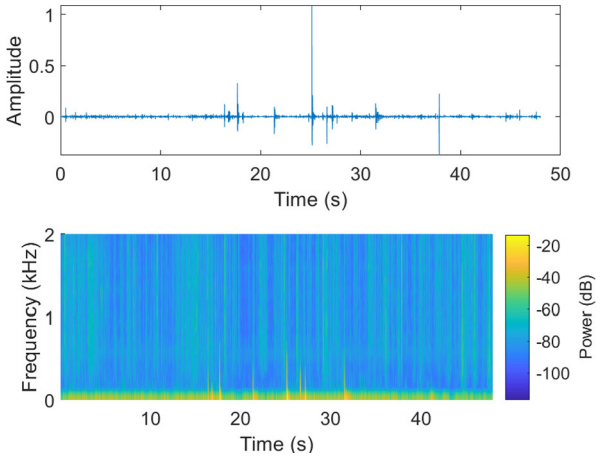

Fig. 17. The time-domain waveform and the corresponding time-frequency analysis result of environmental noise collected in the experiment.

−4 dB. However, the CAS-IUDC-AMSS system using LFM signal needs the SNR above 2 dB to achieve a similar detection probability.

6. Field experiment results

An UWA communication experiment was conducted on the proposed integrated system in Songhua River in December 2020. The system parameters are as follows: the sampling frequency is $f_s = 20$ kHz; The size of waveform train is $M = 8$, $N = 8$, that is, each CAS pulse can carry 3 bits information. The 16 waveforms used in the experiment are the optimized waveforms in Section 5.1. During the experiment, 720 bits binary data is sent with a data rate of 15 bit/s. Fig. 15(a) shows a satellite image of the experiment scenario, where the positions of the transmitter and receiver are marked with green and red dots, respectively. The distance between the transmitter and receiver is about 500 m, and the average water depth is 8 m. Fig. 15(b) shows the specific experiment layout, there is a layer of ice covering the water with a thickness of about 80 cm. The frequency band of the acoustic source is 500 − 2000 Hz. During the experiment, a 5-element hydrophone array is used to receive the UWA signals. The hydrophones are placed at five points A, B, C, D, and E, and the depths are 1 m, 2 m, 3 m, 4 m and 5 m, respectively. The signals they collected are named ES01, ES02, ES03, ES04 and ES05.

Fig. 16 shows the UWA channel estimation results of ES01-ES05. Due to the shallow water depth, the acoustic signals are reflected repeatedly from the surface and bottom in the process of propagation, and multiple channels are mixed together, resulting in a complex multipath channel structure. The multipath delay is roughly 8 ms. Table 2 shows the SNRs of ES01-ES05, which are between 13 and 15 dB. The symbol error rate (SER) results of the proposed integrated system are also listed in Table 2, all receivers can decode correctly. In order to study the communication performance of the proposed CAS-IUDC-AMSS system under low SNR, the

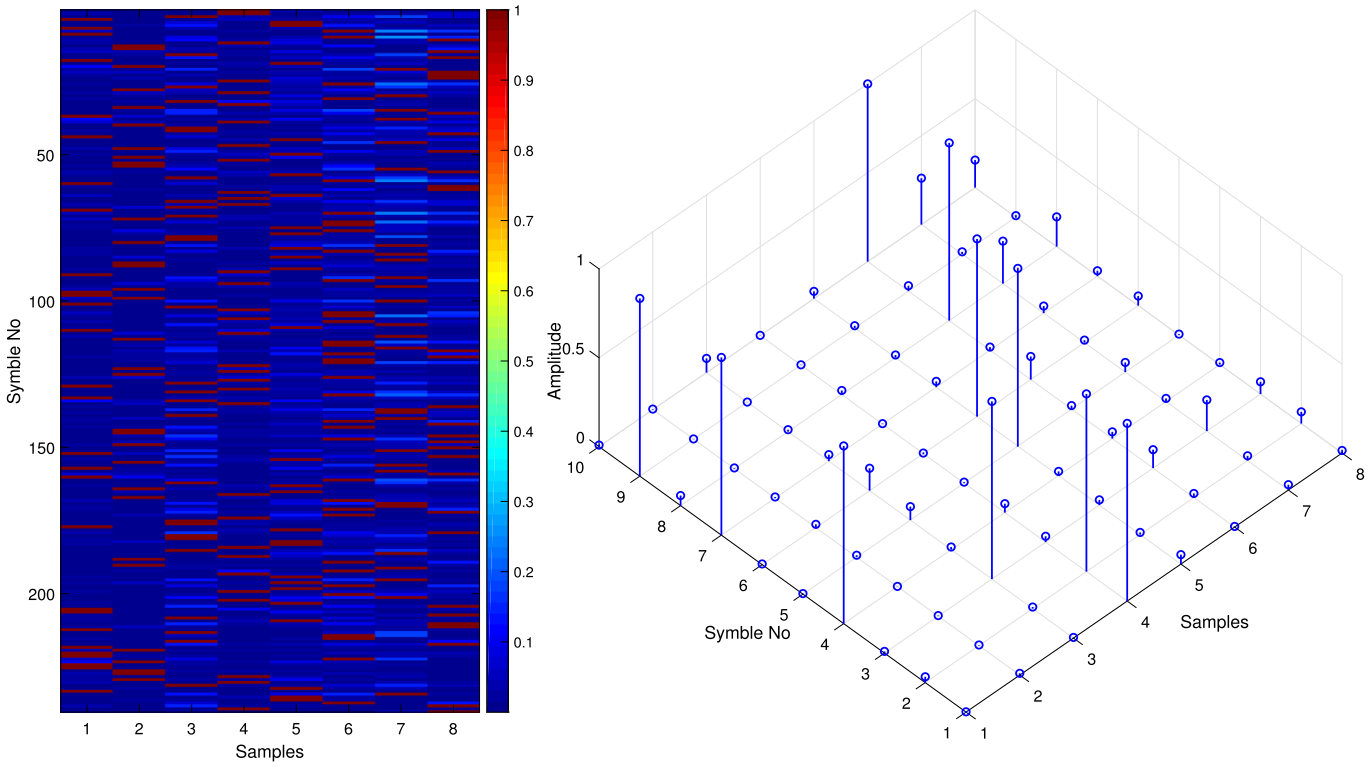

Fig. 18. The energy output result of the MED for (a) all symbols and (b) first ten symbols.

collected environmental noise is artificially added to the received signal to reduce the SNR of the received signal of each element. Fig. 17 shows the time-domain waveform and the corresponding time-frequency analysis result of environment noise collected in the experiment. We adjust the energy of the noise shown in Fig. 17 and add it to the received signals, so that the SNR of the obtained signals is -2 dB. The decoding results are given in Table 2. Except for a symbol error in the #A hydrophone, others can be decoded correctly. Moreover, the CAS-IUDC-AMSS system using sub-band LFM signals is analyzed by artificially superimposing the measured environmental noise and multipath interference of all channels on its transmitted signal. The parameters of sub-band LFM signals are the same as that in the Section 5.2. The decoding results under different SNRs are also listed in Table 2. We find that both systems can decode correctly when the SNR is high, but the CAS-IUDC-AMSS system using sub-band LFM signals has different degrees of decoding errors when the SNR is as low as -2 dB. The analysis results show that the proposed CAS-IUDC-AMSS system using optimized GSFM signals as sub-pulse has superior performance in anti-noise ability and robustness than the system using sub-band LFM signals.

Fig. 18 shows the energy output result of the MED when the ES01 is decoded. Fig. 18(a) is the output result of all symbols, and Fig. 18(b) is the output result of the first ten symbols. It can be seen that when the MED algorithm performs decoding, the energy output peak of each symbol is obvious, so it is not likely to cause misjudgments. This is because we have optimized the CE of the used waveforms in Section 5.1 to reduce their mutual interference in the MED algorithm.

7. Conclusion

In this paper, a novel underwater integrated system of detection and communication based on CAS was proposed. Without affecting the detection performance, the proposed integrated system can carry communication information though AMSS modulation by exploiting the diversity of the waveforms used in active sonar detection. Moreover, to improve the performance of the CAS-IUDC-AMSS system, an optimization approach has been developed for GSFM waveform trains, which is dealt by the GA method. Simulation results indicated that the CAS-IUDC-AMSS system using optimized GSFM signals as sub-pulse has better BER performance and detection performance than using LFM signals. The field experiment results confirm the feasibility and validity of the proposed integrated system in practical applications.

Declaration of competing interest

The authors declare that they have no known competing financial interests or personal relationships that could have appeared to influence the work reported in this paper.

Acknowledgments

This research is supported by the National Natural Science Foundation of China (Grant No. 52071111) and the Ph.D. Student Research and Innovation Fund of the Fundamental Research Funds for the Central Universities (Grant No. 3072021GIP0508).

References

[1] X. Ma, F. Yang, S. Liu, J. Song, Channel estimation for wideband underwater visible light communication: a compressive sensing perspective, Opt. Express 26 (1) (2018) 311–321.
[2] T. Yang, Spatially multiplexed cdma multiuser underwater acoustic communications, IEEE J. Ocean. Eng. 41 (1) (2015) 217–231.
[3] S. Shi, Y. Li, D. Yang, A. Liu, J. Shi, Sparse representation based direction-of-arrival estimation using circular acoustic vector sensor arrays, Digit. Signal Process. 99 (2020) 102675.
[4] S. Majumder, S. Scheding, H.F. Durrant-Whyte, Multisensor data fusion for underwater navigation, Robot. Auton. Syst. 35 (2) (2001) 97–108.

[5] B. Kalyan, A. Balasuriya, Multisensor data fusion approach for terrain aided navigation of autonomous underwater vehicles, in: Oceans' 04 MTS/IEEE Techno-Ocean'04, IEEE Cat. No. 04CH37600, vol. 4, IEEE, 2004, pp. 2013–2018.
[6] J. Yin, W. Ge, X. Han, B. Liu, L. Guo, Partial fft demodulation with irc in mimo-sc-fde communication over Doppler distorted underwater acoustic channels, IEEE Commun. Lett. 23 (11) (2019) 2086–2090.
[7] W. Jiang, F. Tong, S. Zheng, X. Cao, Estimation of underwater acoustic channel with hybrid sparsity via static-dynamic discriminative compressed sensing, IEEE Sens. J. 20 (23) (2020) 14548–14558.
[8] L. Jun, Z. Qunfei, Z. Lingling, S. Wentao, Detection performance of active sonar based on underwater acoustic communication signals, in: 2018 IEEE International Conference on Signal Processing, Communications and Computing (ICSPCC), IEEE, 2018, pp. 1–5.
[9] Y. Liu, G. Liao, Z. Yang, J. Xu, Multiobjective optimal waveform design for ofdm integrated radar and communication systems, Signal Processing.
[10] W. hua Wu, Y. he Cao, S. hua Wang, T.-S. Yeo, M. Wang, Mimo waveform design combined with constellation mapping for the integrated system of radar and communication, Signal Process. 170 (2020) 107443, https://doi.org/10.1016/j.sigpro.2019.107443.
[11] S. Shi, Z. Wang, Z. He, Z. Cheng, Constrained waveform design for dual-functional mimo radar-communication system, Signal Process. 171 (2020) 107530, https://doi.org/10.1016/j.sigpro.2020.107530.
[12] M. Jiang, G. Liao, Z. Yang, Y. Liu, Y. Chen, Integrated radar and communication waveform design based on a shared array, Signal Process. 182 (1) (2020) 107956.
[13] J. Yin, W. Men, X. Han, L. Guo, Integrated waveform for continuous active sonar detection and communication, IET Radar Sonar Navig. 14 (9) (2020) 1382–1390.
[14] G. Hickman, J.L. Krolik, Non-recurrent wideband continuous active sonar, in: 2012 Oceans, IEEE, 2012, pp. 1–6.
[15] S.M. Murphy, P.C. Hines, Sub-band processing of continuous active sonar signals in shallow water, in: OCEANS 2015, Genova, 2015, pp. 1–4.
[16] A. Munafò, G. Canepa, K.D. LePage, Continuous active sonars for littoral undersea surveillance, IEEE J. Ocean. Eng. 44 (4) (2018) 1198–1212.
[17] D.A. Hague, J.R. Buck, The generalized sinusoidal frequency-modulated waveform for active sonar, IEEE J. Ocean. Eng. 42 (1) (2016) 109–123.
[18] D.A. Hague, J.R. Buck, The generalized sinusoidal frequency modulated waveform for high duty cycle active sonar, in: 2014 48th Asilomar Conference on Signals, Systems and Computers, IEEE, 2014, pp. 148–152.
[19] D.A. Hague, J.R. Buck, The generalized sinusoidal frequency modulated waveform for continuous active sonar, in: OCEANS 2015-Genova, IEEE, 2015, pp. 1–8.
[20] W.-B. Yang, T. Yang, High-frequency channel characterization for m-ary frequency-shift-keying underwater acoustic communications, J. Acoust. Soc. Am. 120 (5) (2006) 2615–2626.
[21] F. Zhou, B. Liu, D. Nie, G. Yang, W. Zhang, D. Ma, M-ary cyclic shift keying spread spectrum underwater acoustic communications based on virtual time-reversal mirror, Sensors 19 (16) (2019) 3577.
[22] Y. Doisy, L. Deruaz, S.P. van IJsselmuide, S.P. Beerens, R. Been, Reverberation suppression using wideband Doppler-sensitive pulses, IEEE J. Ocean. Eng. 33 (4) (2008) 419–433.
[23] G. Rui, W. Xiao-tong, C. Zhi-ming, Comparison research on reverberation strength excited by ptfm and cw signals, in: 2016 IEEE 13th International Conference on Signal Processing (ICSP), IEEE, 2016, pp. 1677–1681.
[24] B. Liu, J. Yin, G. Zhu, An active detection method for an underwater intruder using the alternating direction method of multipliers, J. Acoust. Soc. Am. 146 (6) (2019) 4324–4332.
[25] H. Hu, B. Liu, Genetic algorithm for designing polyphase orthogonal code, in: 2008 4th International Conference on Wireless Communications, Networking and Mobile Computing, IEEE, 2008, pp. 1–4.
[26] C. Guan, Z. Zhou, X. Zeng, Optimal waveform design using frequency-modulated pulse trains for active sonar, Sensors 19 (19) (2019) 4262.
[27] H. Tamaki, H. Kita, S. Kobayashi, Multi-objective optimization by genetic algorithms: a review, in: Proceedings of IEEE International Conference on Evolutionary Computation, IEEE, 1996, pp. 517–522.

Wei Men received the B.S. degree from the College of Underwater Acoustic Engineering, Harbin Engineering University, Harbin, China, in 2018, where he is currently pursuing the Ph.D. degree with the College of Underwater Acoustic Engineering. His research is interested in underwater acoustic communication and detection.

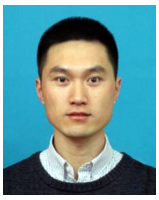

Liang Zhang received the M.E. degree in underwater acoustic engineering, and the Ph.D. degree in information and communication engineering from Harbin Engineering University, Harbin, China, in 2010 and 2016, respectively. From September 2013 to June 2014, he was a Visiting Ph.D. Student with the University of Victoria, Victoria, BC, Canada, and from July 2014 to September 2015, he was a Visiting Ph.D. Student with McMaster University, Hamilton, ON, Canada.

In 2019, he joined the School of Information and Control Engineering, China University of Mining and Technology, Xuzhou, China, where he was a Lecturer. Since 2020, he has been with the College of Underwater Acoustic Engineering, Harbin Engineering University, where he is currently an associate professor. His research interests include array processing, robust beamforming, and numerical optimization with applications to radar and sonar.

Jingwei Yin received the B.S., M.S., and Ph.D. degrees in underwater acoustic engineering from the Harbin Engineering University, China in 1999, 2006, and 2007, respectively.

He is currently a Visiting Professor with the Russian Far Eastern Federal University. He is also a Professor of the College of Underwater Acoustic Engineering, Harbin Engineering University, China. He is also the Deputy Director of the Water Acoustic Branch, China Acoustic Society. He is also the Director of the Key Laboratory of Marine Information Acquisition and Security, Harbin Engineering University, Ministry of Industry and Information Technology. He has published a monograph, over 100 papers, and over 20 inventions. His current research interests include underwater acoustic engineering, underwater acoustic communication, and polar acoustics.

Jiaqi Wang received the B.S. degree from the College of Underwater Acoustic Engineering, Harbin Engineering University, Harbin, China, in 2019, where he will receive the M.S. degree in 2022. His research interest is the integration of sensing and communication.